Surveys of Geophysics manuscript No.
(will be inserted by the editor)

Response of a Coupled Ocean-Atmosphere Model to Greenland Ice Melting

D. Stammer · N. Agarwal · P. Herrmann · A. Köhl · C.R. Mechoso

Received: date / Accepted: date

Abstract Keywords Greenland ice sheet melting · sealevel rise · coupled atmosphere-ocean experiments

D. Stammer

Institut für Meereskunde

Universität Hamburg, Germany

Tel.: +49-40-428385052

Fax: +49-40-428387063

E-mail: detlef.stammer@zmaw.de

N. Agarwal and P. Herrmann

Max-Planck-Institut für Meteorologie, Hamburg, Germany

A. Köhl

Institut für Meereskunde, Universität Hamburg, Germany

C.R. Mechoso

University of California, Los Angeles, USA

We investigate the transient response of the global coupled ocean-atmosphere system to enhanced freshwater forcing representative of melting of the Greenland ice sheets. A 50-year long simulation by a coupled atmosphere-ocean general circulation model (CGCM) is compared with another of the same length in which Greenland melting is prescribed. To highlight the importance of coupled atmosphere-ocean processes, the CGCM results are compared with those of two other experiments carried out with the oceanic component of the coupled model (OGCM). In one of these OGCM experiments the prescribed surface fluxes of heat, momentum and freshwater correspond to the unperturbed simulation by the CGCM; in the other experiment Greenland melting is added to the freshwater flux. The responses by the CGCM and OGCM to the Greenland melting have similar patterns in the Atlantic, albeit the former have five times larger amplitudes in sea surface height anomalies. The CGCM shows likewise stronger variability in all state variables in all ocean basins because the impact of Greenland melting is quickly communicated to all ocean basins via atmospheric bridges. We conclude that the response of the global climate to Greenland ice melting is highly dependent on coupled atmosphere-ocean processes. These lead to reduced latent heat flux into the atmosphere and an associated increase in net freshwater flux into the ocean, especially in the subpolar North Atlantic. The combined result is a stronger response of the coupled system to Greenland ice sheet melting.

1 Introduction

As a community, we are gradually coming closer to a better understanding of the present-day global sea level budget. However, many questions remain open on the subject of sea level variability and changes on regional scale and their future projection under climate change conditions. This situation is partly due to the large uncertainties of contemporary climate models in successfully reproducing the variability of the current climate. The lack of representation in the models of all forcing components of the climate system is an important contributor to such uncertainty. In this regard, a big deficit exists in the detailed knowledge of the impacts on regional sea level of freshwater input into the high-latitude oceans originating from the melting polar ice sheets.

Emerging knowledge suggests that sea level changes resulting from polar ice sheet melting are far from being intuitive. Instead, these changes seem to be associated with a strong regional dynamical response superimposed on contributions originating from the solid earth. For example, Stammer (2008), using an ocean-only general circulation model (OGCM), highlighted the transient, steric (i.e., due to thermal expansion or haline contraction) response of the global ocean circulation to localized freshwater forcing around Greenland. In that study, increased freshwater runoff from Greenland resulted in a basin-wide steric response on timescales of a few years. The response was communicated remotely via oceanic processes including boundary waves, equatorial Kelvin waves, and propagating baroclinic Rossby waves. On the basis of those results, Stammer (2008) speculated that consideration of coupled atmosphere-ocean processes might significantly modify the insights obtained in an ocean-only framework. Hu et al. (2009) recently addressed some aspects of the coupled ocean-atmosphere response to potential Greenland ice sheet melting during the 21st century. In this case, the approach was based on the Community Climate System Model version 3 (CCSM3), and the transient response of the meridional overturning circulation (MOC) was emphasized. The paper suggests that only a strong ice sheet melting flux and associated net freshwater gain in the upper subpolar North Atlantic can weaken the MOC, but that the weakened MOC subsequently reduces the magnitude of the warming in the northern high latitudes by a few degrees, which in turn influences the regional sea level there. Using a different coupled ocean-atmosphere model (CGCM), Okumora et al. (2009) investigated the mechanisms by which a large freshwater input into the subarctic North Atlantic can influence the North Pacific climate via both oceanic and atmospheric pathways. The oceanic teleconnection contributes a large part of the North Pacific cooling through the Bering Strait throughflow by transporting colder, fresher water from the Arctic Ocean into the North Pacific. In addition, an atmospheric bridge originating from the North Atlantic leads to modified surface heat fluxes and southward Ekman transport in the Pacific, thereby playing a crucial role in the teleconnection between ocean basins.

Obviously the subjects of regional sea level variability and change in response to Greenland ice sheet melting warrant more investigations and discussions. Of special concern are the feedback mechanisms and intrinsic time scales in the coupled climate system to freshwater input from polar ice sheets. In this context, the following questions need to be addressed:

1. What are the basin-wide responses of the ocean and atmosphere to increased melting of the polar ice sheets during the first decades after its onset?
2. How important are coupled atmosphere-ocean processes for the ocean's response to Greenland ice sheet melting, and what are those air-sea feedback mechanisms?
3. What is the role played by atmospheric and oceanic pathways in forcing the Pacific and Indian Oceans, what are the detailed paths, and how fast is the global response?

The present study addresses these questions by contrasting the oceanic response to increased melting of Greenland ice masses in a numerical model of the coupled atmosphere-ocean system with that obtained using the ocean component of the model with prescribed boundary conditions. The focus is on aspects related to changes in sea surface height (SSH). The special mechanisms at work in the response of the coupled system to perturbations in the ocean around Greenland and the pathways of anomalies in the atmosphere into the Pacific and Indian Ocean will be analyzed elsewhere (Agarwal et al., 2011).

The structure of the paper is as follows: Section 2 introduces the models used and describes the integrations performed. Section 3 compares the SSH response obtained in the model experiments. Section 4 discusses differences of the SSH responses obtained in the coupled framework relative to those emerging from the ocean-only run. Section 5 concentrates on changes of the MOC and polar heat transports in the Atlantic. Section 6 presents a discussion and the concluding remarks.

2 The Model Set-up and Experiments

Our study is based on the University of California, Los Angeles (UCLA) CGCM consisting of the UCLA atmospheric general circulation model (AGCM) coupled to the Massachusetts Institute of Technology (MIT) oceanic general circulation model (OGCM). Cazes-Boezio et al. (2008) describe the model's performance in the context of El Niño/Southern Oscillation (ENSO) forecasts. Details about the model are reported in Ma et al. (2010), and are also available online at http://www.atmos.ucla.edu/mechoso/esm/agcm.html.

The AGCM is a state-of-the-art model with advanced parameterizations of the major atmospheric physical processes. The parameterization of cumulus convection, including its interaction with the planetary boundary layer (PBL), follows the prognostic version of Arakawa and Schubert (1974) according to Pan and Randall (1998). The model includes parameterizations of prognostic cloud liquid water and ice (Köhler 1999). The parameterization of PBL processes is based on the mixed-layer approach of Suarez et al. (1983), as revised by Li et al. (2002), and upgraded to multi-layer by Konor et al. (2008). The parameterization of radiation processes is based on Harshvardhan et al. (1987; 1989), and includes the effects of cumulus, ice and PBL clouds.

In the present study, we use AGCM version 7.1 with a horizontal resolution of 2.5° longitude and 2° latitude, and 29 layers in the vertical. Beginning with this version, the AGCM is coupled to the first-generation Simplified Simple Biosphere model (SSiB; Xue et al., 1991). In this model several sources of data (Dorman and Sellers, 1989; Xue et al., 1996a, 1996b) are used to determine the vegetation types that specify monthly climatological land surface properties (e.g., leaf area index, green leaf fraction and surface roughness length). The distributions of greenhouse gases, sea ice, and ocean surface albedo are all prescribed corresponding to a monthly-mean observed climatology. SSiB has three soil layers and one vegetation layer.

The OGCM domain is quasi-global (80°S to 80°N) with all lateral boundary conditions closed. The sea-ice distribution is prescribed according to an observed monthly climatology. In our application, the zonal grid spacing in the MIT OGCM is 1° of longitude. The meridional ocean grid spacing is 0.3° of latitude within 10° of the Equator and increases to 1° latitude poleward of 22°N and 22°S. There are 46 ocean levels with thicknesses ranging from 10 m in the top 150 m, and gradually increasing to 400 m thickness near the maximum model depth of 5815 m. The model's bathymetry is based on ETOPO5 (Data Announcement 88MGG-02, Digital relief of the Surface of the Earth, NOAA, National Geophysical Data Center, Boulder, Colorado, 1988). The model employs the K-Profile Parameterization (KPP) vertical mixing scheme of Large et al. (1994) and the isopycnal mixing schemes of Redi (1982) and of Gent and McWilliams (1990) with surface tapering as per Large et al. (1997). Laplacian diffusion and friction are used except that horizontal friction is biharmonic. No-slip bottom, free-slip lateral, and free surface boundary conditions are employed. Surface freshwater fluxes are applied as virtual salt fluxes and heat and freshwater fluxes are exchanged between the ocean and the atmosphere at an interval of 1 day. Isopycnal diffusivity and isopycnal thickness diffusivity is $500m^2s^{-1}$. Vertical diffusivity is $5 \times 10^{-6}m^2s^{-1}$. Horizontal and vertical viscosities are $1013m^4s^{-1}$ and $10^{-4}m^2s^{-1}$, respectively.

As a preliminary step, the CGCM model was spun up for 30 years. The initial conditions for the AGCM correspond to November 1 in a long climate run with distribution of sea surface temperature corresponding to an observed climatology. The initial conditions for the OGCM correspond to the climatological temperature and salinity fields for November from Levitus et al. (1994). Initial conditions for all subsequent runs were taken from the end of the 30-year spin up. Using these initial conditions, the following set of experiments was performed, each lasting for 50 years:

1. The CGCM was integrated forward in time. This model integration will be referred to as the unperturbed coupled run.
2. The CGCM was integrated forward again, using exactly the same initial conditions as used in the unperturbed coupled run, but this time with a freshwater perturbation applied around Greenland as a virtual salt flux. This will be referred to as the perturbed coupled run.

The freshwater perturbation is 0.0275 Sv (1 Sv = $10^6m^3/s$, equivalent to about 2 mm/yr global sea level increase), five times the size of the present day estimated sea-ice melting rates (0.0055 Sv; Luthke 2006), and its spatial distribution is shown in Fig. 1. The factor of five was applied to obtain a response with a magnitude larger than the model's internal variability. With this prescribed Greenland runoff, the ocean model response is comparable to that in Stammer (2008) in amplitude (see below). In contrast to that study, however, the surface temperature and salinity in our runs are not relaxed toward climatological fields. The magnitude of freshwater input obtained in this way is still an order of magnitude smaller than the hysteresis width reported by Rahmstorf et al. (2005), and more than 30 times smaller than the 1 Sv prescribed in typical water-hosing experiments (e.g., Timmermann et al., 2007; Stouffer et al, 2006).

To analyze the impact of coupling, two additional model integrations were performed, using the ocean component of the CGCM, again run over 50 years using the surface flux fields diagnosed from the unperturbed coupled run and starting from the same initial conditions as the coupled runs:

1. The OGCM was integrated forward in time, using the heat and freshwater fluxes obtained from the unperturbed coupled run. This model integration will be referred to as the ocean-only unperturbed run.
2. The OGCM was integrated forward in time again using the initial conditions of the ocean-only unperturbed run and with the same additional freshwater OGCM input around Greenland prescribed as a virtual salt flux in the coupled run. This model integration will be referred to as the ocean-only perturbed run.

Fig. 2

To investigate the response of the ocean-only or the coupled models to Greenland meltwater forcing, we focus the further analysis on the differences between perturbed and unperturbed coupled and ocean-only runs. For convenience, we will refer to those twin runs as the coupled experiments and the ocean-only experiments. However, to avoid analyzing climate noise originating from perturbations in the initial state rather than signals originating from the freshwater perturbations around Greenland, we will in the following analyze only lowpass filtered differences between the reference runs and the perturbed runs. In addition, we will average those differences in time and or space to further reduce any potential contamination from climate noise. To put later results into context, we show in Fig. 2 the standard deviation (STD) of the lowpass filtered SSH in the unperturbed coupled run. From the figure it follows that the Atlantic and the Southern Ocean of the coupled reference run both show interannual to decadal variability of the order of 10 cm; respective numbers appear to be lower than 5 cm in the Indian Ocean and are even smaller over large parts of the Pacific.

A special feature of this paper is that the initial conditions in our experiments do not correspond to the model's longterm equilibrium state, since the 30-year spin-up of the CGCM is not long enough to achieve such a state. We can expect an extra model drift to be added resulting from the freshwater forcing. However, by not running the coupled model into equilibrium we intend the ocean state to remain close to the observed observed climatology. In this way, the propagation of perturbations applied at the ocean's surface (such as freshening) into the interior basins will be more realistic than it would be through an equilibrium ocean state of the CGCM affected by the model's systematic errors.

3 Sea Surface Height Anomalies

Lowpass filtered SSH anomalies (i.e., differences between the values in the perturbed and the unperturbed runs) obtained in the ocean-only experiments are shown in left column of Fig. 3 after averaging them over the periods years 6 Fig. 3
- 10, years 26 - 30, and years 41-45, respectively. Overall, the response agrees well with results obtained from Stammer (2008) (both in amplitude and pattern) and shows similar spatial patterns characterized by negative anomalies in the central North Atlantic and positive anomalies propagating southward. Associated steric anomalies reach amplitudes of about 4 cm along the western coast of the North Atlantic after just a few years, and basin-scale steric anomalies of about 1 cm in the North Atlantic after 30 years. In contrast, SSH anomalies are only about 1 mm in the Pacific (see also below).

For a comparison we show in the right column of Fig. 3 similar SSH anomalies, but from the coupled experiment. There are several outstanding differences between the results in the experiments. Firstly, in the coupled experiment, clear SSH anomalies over the global ocean are evident in all three panels, with spatial patterns that are approximately the same scale and amplitude in the Indian Ocean and the Pacific. Moreover, in the Atlantic we find again structures similar to those obtained by Stammer (2008); however, the magnitude of the anomalies in the coupled experiment is substantially larger than in the ocean-only case. In the former experiment, the averaged steric increase in the Atlantic comes close to 1 cm in the first years and exceeds 10 cm in the lowest panel. We conclude from Fig. 3 that coupled processes do not significantly alter the SSH response in the Atlantic in terms of pattern but increase the magnitudes by a factor of about 5. In addition, the coupled experiment shows clear and statistically significant responses in all other ocean basins. These are of gyre-scale, suggesting that they essentially represent adjustments of the ocean circulation to changes of the atmospheric forcing in those basins. In particular, the negative SSH anomaly in the northern North Pacific has amplitudes that exceed the natural climate noise by several STDs.

Fig. 4

The time evolution of steric SSH anomalies averaged over the different ocean basins are shown in Fig. 4 for the coupled and ocean-only experiments. The values in Fig. 4 were corrected for the Boussinesq approximation effect on the global volume (Greatbatch 1994). According to Fig. 4, the SSH increase in the ocean-only experiment is largest in the North Atlantic, followed by the South Atlantic with about 50% of the amplitude. The increases in both the Indian Ocean and the Pacific are only about 25% of those in the North Atlantic. In all basins, the increase is smooth and almost monotonic in time, reaching about 1.5 cm in year 30 in the North Atlantic (2 cm in year 50) and about 0.5 cm in the North Pacific. In the coupled experiment, the largest SSH increase is also in the North Atlantic, while the increase in all other basins is substantially smaller, such that the long-term response in the South Atlantic is still larger than in the Pacific and the Indian Ocean. The increase in the North Atlantic reaches 8 cm during year 50, 3 cm in the South Atlantic, and about $1-2$ cm in the North Pacific and Indian Ocean. Moreover, we note that the SSH varies strongly in all basins on interannual to decadal time scales, and that superimposed on those pronounced basin-scale oscillations in the coupled Pacific and Indian Ocean, both oceans show a net increase in steric sea level. In all basins and even as a global average, the SSH response in the coupled experiment is stronger than in the ocean-only one.

Figure 4 also shows in both panels as a blue dashed line the response of the global non-steric SSH increase due to the volume of melt water added to the ocean. These results illustrate that, in contrast to the ocean-only run experiment in which the non-steric SSH increase directly related to the Greenland melt is substantially larger than the steric response, the steric response in the coupled experiment has comparable order of magnitude in the North Atlantic. Two reasons as demonstrated below are responsible for this. Firstly, the atmospheric response contributes additional freshwater leading to a 76% larger halosteric increase (i.e., the volume increase due to freshening of the water column). Secondly, the associated heating and cooling patterns lead to a stronger heating in warm regions with relatively larger thermal expansion and stronger cooling in colder regions with smaller thermal expansion.

4 On the Different Responses in the Coupled and Ocean-Only Experiments

Fig. 5

To investigate why steric responses are stronger both regionally, and globally (by a factor of about 2) in the coupled experiment, we compare in Fig. 5 the thermosteric and halosteric contributions to steric sea level change in the two experiments. The figure reveals that both contributions are larger in the coupled experiment as would result from enhanced surface heat and net freshwater input into the ocean. Nevertheless, the thermosteric component is still the main contributor to stronger steric SSH increase in the coupled experiment. The same component is also responsible for the pronounced temporal variability in the steric response. This result highlights again the coupled nature of the response of the climate system to Greenland meltwater forcing.

Fig. 6

Fig. 7

The time series of basin averaged SSH anomalies and the relative contributions from the thermosteric and halosteric components are shown in Fig. 6 and Fig. 7 for the ocean-only and coupled experiments, respectively. The results for the North Atlantic, the South Atlantic, the Pacific, and the Indian Ocean are shown separately. In both cases, thermosteric anomalies dominate the SSH increases in all basins, albeit with much larger amplitudes in the coupled experiment. An exception is the North Atlantic, however, where the net SSH response in the ocean-only experiment is smaller than what would result from the halosteric component alone due to a negative thermosteric contribution. In contrast, the North Atlantic warms while becoming fresher in the coupled experiment, which leads to a much larger increase in basin-scale sea level. We also note the generally stronger, and temporally more variable halosteric response in all basins in the coupled experiment. We note that - in the absence of any additional surface heat fluxes - the thermosteric effect in the ocean-only experiment can only result form the redistribution of heat by the changing circulation, the altered convection and the associated heating or cooling of near-surface water with different temperature than available in the unperturbed reference run.

To examine the causes for the enhanced steric response in the coupled experiment, we show in Fig. 8, as an example, the mean lowpass filtered salinity anomalies at 160 m depth from both experiments, averaged over the periods years 6-10, years 26-30, and years 41-45, respectively. The corresponding temperature anomalies are shown in Fig. 9. In the ocean-only experiment the response has a similar pattern to that obtained by Stammer (2008); e.g., positive temperature anomalies appear around the coast of Greenland in year 1, subsequently move southward along the western coast of North America and later on spread across the equator via Kelvin waves. In the coupled experiment, the fields displayed in Fig. 8 and Fig. 9 show temperature and salinity perturbations stronger by an order of magnitude and include a pronounced remote response (in the Indian Ocean and Pacific) already during the first year. A remote response of comparable magnitude is totally absent in the ocean-only run. Such a quick and strong baroclinic response cannot be explained by ocean dynamics only. The signal must be transmitted by the atmosphere in response to the sea surface temperature (SST) anomalies in the subpolar

Fig. 8

Fig. 9

North Atlantic. We see that the subtropical gyres of all basins are dominated in the coupled run by basin-scale positive and negative anomalies that increase in amplitude and shift laterally with time. The pattern of the anomalies, however, does not change fundamentally with time, which is a typical forced ocean variability pattern.

Fig. 10
Fig. 11

The mean temperature anomalies averaged over the 50-year period of the ocean-only and coupled experiments are depicted in Fig. 10 and 11 along two meridional sections at 30°W and 180°E, respectively. In the ocean-only experiments, negative perturbations are maximum in the subpolar North Atlantic, where they extend throughout the entire ocean column. There are weaker negative anomalies over the Southern Ocean, while positive anomalies characterize the subtropics. Interestingly, a similar meridional distribution of temperature anomalies can be observed in the Pacific, albeit with much reduced amplitudes. The situation is again substantially different in the coupled experiments. Here we find positive and negative anomalies with typically gyre scale in both hemispheres. Moreover, the surface layer has cooled in most of the two sections.

Fig. 12

The temperature and salinity anomalies discussed in the previous paragraph are associated with anomalies in heat and freshwater contents. Averaged over the 50-year long run, the vertically integrated freshwater anomaly in the subpolar North Atlantic is generally positive (Fig. 12a), as expected since freshwater was added as runoff around Greenland. Other parts of the World Ocean also experience freshening, notably the South Atlantic and the South Pacific. In contrast, salinity increases in the tropical Atlantic, parts of the Indian Ocean, and in large areas of the Pacific and the Southern Ocean. Turning to the vertically integrated heat content (Fig. 12b), changes are to some extent consistent in pattern with density compensated freshwater changes as they would result from changes in the ocean circulation and an associated redistribution of heat and freshwater (see also Pardaens et al., 2010, and Landerer et al., 2007, for respective result in coupled climate scenario runs). A clear exception is the North Atlantic, where a positive heat anomaly is obvious along the entire western boundary.

The changes in freshwater and heat content shown in Fig. 12 are associated with, to some extent, changes in the net surface freshwater and heat fluxes shown in Fig. 13. According to this figure, on top of the addition of freshwater from Greenland melting, the net surface freshwater flux into the ocean (Fig. 13a) is further enhanced along the western boundary of the North Atlantic as well as over large parts of the tropics. In contrast, the freshwater flux into the ocean is reduced in the Intertropical Convergence Zones (ITCZ) regions of all oceans. The changes in the net surface freshwater flux in the coupled experiment are largely related to surface temperature dependent evaporation changes, which are directly related to changes in latent surface heat flux (Fig. 13b). This is especially clear in the western North Atlantic, where in response to the Greenland freshwater perturbation, the latent heat flux into the atmosphere is substantially reduced (Fig. 13c), resulting in enhanced freshwater input into the ocean. At the same time, sensible heat flux and long wave radiation into the atmosphere are reduced as well. Likewise, the net increase of

Fig. 13

heat flux into the atmosphere in the eastern North Atlantic (and the Kuroshio region) is also caused by changes in the latent and sensible heat flux. Finally, over the entire tropical oceans, changes in the latent heat are associated with local variations in net freshwater fluxes. However, we also observe changes in the shortwave radiation both in the tropics and in the North Atlantic, as they would result from changes in the cloud coverage.

Breaking down the global surface freshwater flux variations over the ocean in terms of changes in evaporation and precipitation, we find that these decrease by about 0.0116 Sv and 0.0272 Sv, respectively. The two effects combined lead to a net increase in freshwater input into the ocean by 0.0156 Sv in the coupled experiment as compared to the ocean-only experiment. This is on top of the added 0.0275 Sv Greenland runoff, which leads to a global net reduction in freshwater flux (E-P-R) = 0.0156+0.0275 = 0.0431 in the coupled experiment. This net freshwater input results in an increase in the halosteric SSH anomaly, largely due to a reduction in evaporation rather than an increase in precipitation. At the same time the reduced evaporation is a net heat source for the ocean, which again is consistent at least partially with the increased thermosteric increase in sea surface height. Both processes are especially active in the North Atlantic, where they play an essential role in the larger steric SSH response of the coupled experiment. Acting concurrently, they provide an additional source of buoyancy in the subpolar North Atlantic in the coupled model with consequences for the ocean circulation.

We note that in our model the additional freshwater is being taken out of the soil moisture. Over a 50-year period it appears as a plausible response of the coupled climate system given that it corresponds to only about 1% of the global river run-off into the ocean. However, such an additional freshwater source cannot be sustained in long climate scenario runs and it remains to be investigated how the global water cycle of the climate system would adjust in long climate scenario runs.

5 Impacts on the Atlantic MOC and Meridional Heat Transport

Changes in the meridional overturning circulation (MOC), represented here by the meridional overturning streamfunction, and the meridional heat transport in the Atlantic illustrate both succinctly and in a dynamically compact way the complex ocean response to the Greenland freshwater forcing as expressed in the differences in the coupled and ocean-only experiments (Fig. 14). In the Fig. 14
former case, the MOC weakens by about 1.5 Sv – i.e., by about 10% – at 50°N in year 8; the tendency to decrease is apparent over the entire North Atlantic. The coupled experiment shows a similar tendency to MOC decrease (Fig. 14b). However, in this case there are also pronounced positive and negative values in low latitudes and over the Southern Ocean as they would result from changes in the regional circulation, which points again to a role for the atmosphere in generating remote responses in the gyre scale.

To illustrate the temporal behavior of the MOC in the ocean-only and coupled experiments, we show in Fig. 15 time-latitude plots at 1000 m depth. Fig. 15

The former case shows a clear oscillatory behavior of the MOC strength with roughly decadal periodicity, superimposed on a longer-term decline. Anomalies tend to propagate southward from the subpolar Atlantic basin, as in the results of Stammer (2008). We recall that results shown in the present paper follow from a purely flux-driven run without a relaxation term included in the surface boundary conditions. The coupled experiment shows a far more complex evolution of MOC anomalies, which includes interannual fluctuations superimposed on decadal variations that appear somewhat weaker than in the ocean-only experiment. Both are superimposed on a quite pronounced longer-term reduction of the MOC by about 5 Sv over the 50-year length of the integrations.

The variations in the MOC shown in Fig. 15 are associated with variations in the meridional heat transport, which in the uncoupled experiment show a similar oscillatory behavior with increasing amplitude but generally negative tendency (Fig. 16. In the coupled experiment reduction of northward transport of heat is up to 0.2 PW over the 50-year period in the North Atlantic. Superimposed on these longer-term reductions are interannual to decadal variations.

Fig. 16

Oscillations resembling those in Figs. 15 and 16 were found by Eden and Greatbatch (2003) in coupled and uncoupled model configurations, and were associated with patterns of a north-south temperature dipole, similar to those shown here in Fig. 12. These authors found stronger oscillations in the coupled configuration due to a positive feedback via the wind driven circulation.

A delayed negative feedback via the overturning circulation enables the oscillation. In the subpolar region north of 40°N the propagation speed of the anomalies in heat transport anomalies in the ocean-only experiment appear to be much faster than those in the MOC, indicating a fast response of the subpolar gyre circulation. In year 40, for example, the positive heat transport anomaly is associated with a negative delayed response of the MOC anomaly similar to findings by Eden and Greatbatch (2003). In contrast to their results, however, our coupled experiment shows a weaker decadal oscillation than the ocean-only one, but a much stronger longterm trend. Due to a positive feedback with the atmosphere, the anomalies become more negative with time, reaching extremes of 11 -14 Sv during the last 5 years of the integration.

In both experiments, the freshwater anomaly around Greenland causes a reduction in overturning, which in turn causes less transport of heat and salt from the Equator to the subpolar North Atlantic, resulting in a dipole for salinity and temperature. However, only in the coupled experiment, according to the temperature dependence of the heat flux terms, the local heat flux out of the ocean is reduced, especially through the latent heat flux. Along with marginal reduction in the wind speed this causes also a lower rate of latent heat flux than that prescribed in the ocean-only experiment, which results in freshening and warming of the Labrador Sea (seen as stronger thermo- and halosteric responses above), which in turn provides a positive feedback in reducing the MOC.

This type of feedback is known to cause much larger responses in the ocean in terms of MOC changes as compared to a flux driven ocean model (e.g., Rahmstorf and Willebrand, 1995). The mechanism seems to be strong enough in our experiment (given the strength of the applied perturbation) to reduce the decadal oscillations. Instead, variations on a much longer time scale become dominant which may cause the stronger trend in the coupled experiment. We note here that this trend is not continued beyond year 50 (not shown) suggesting it to be part of a longer term oscillation. Whether this is the case or a result of the model not being in a statistical equilibrium is not clear at this point and it will be addressed in the study of Agarwal et al. (2011).

6 Concluding Remarks

The present paper extends the earlier study of Stammer (2008) by investigating now regional sea level changes in response to enhanced Greenland ice mass loss using the same ocean model both uncoupled and coupled to a general circulation model of the atmosphere. Similar to the previous ocean-only results, we also find strong variations in regional sea level in the coupled system. However, in contrast to the ocean-only model experiment, the coupled one produces a stronger and faster response in steric height in the Pacific and Indian Ocean than that obtained by in the OGCM by considering ocean processes only. We find, therefore, that the atmosphere seems to play an additional and prominent role in causing sea level variations in all parts of the World Ocean on short time scale.

Okumora et al. (2009) reported the existence of an atmospheric bridge from the tropical Atlantic into the Pacific, leading to long-term changes in the Pacific and Indian Ocean. Here we show that such a bridge is initially triggered by interactions between the atmosphere and ocean in the subpolar Atlantic, where SST anomalies develop. On both the global and basin scale we see a stronger response of the steric SSH in the coupled system, which is primarily due to a stronger thermal response. This strengthening results from feedbacks between the perturbed ocean (by Greenland freshwater run-off) and the overlying atmosphere, which leads to reduced SSTs in the subpolar North Atlantic, less evaporation and less latent heat flux into the atmosphere. These processes then lead to a local increase in heat content and freshwater content and on global scale result in a steric SSH increase. In the North Atlantic the steric increase is comparable to the non-steric increase caused by the addition of freshwater from Greenland ice mass loss. A detailed examination of these coupling processes will be performed in Agarwal et al. (2011) where we will also investigate the sensitivity of the response to the detailed state of the CGCM.

We note that the patterns obtained in the surface heat and freshwater fluxes of the North Atlantic resemble surprisingly well those reported by Hawkins and Sutton (2009) in terms of optimal perturbations in the Atlantic. Their optimal perturbation pattern showed that the HadCM3 CGCM is highly sensitive to small perturbations in temperature around Greenland, anticipating that any perturbation in SST resulting from Greenland freshwater pulses would have a substantial effect on the coupled system. We find a similar sensitivity in our results, suggesting the presence of strong and direct interaction mechanisms between the ocean and the atmosphere in response to SST changes in the subpolar North Atlantic. In our case it is caused by the addition of Greenland freshwater melting; however, the mechanism should hold more generally for any SST anomaly present in the subpolar North Atlantic and potentially can have a large consequence for our understanding of the geographical distribution of air-sea coupling and the way the ocean is influencing the atmosphere.

Our results clearly support the notion that it is important to properly consider the effects of freshwater sources resulting from polar ice sheet melting in coupled climate models, so as to successfully simulate the feedback mechanisms between the ocean and the atmosphere thereby improving projections of the climate, including regional sea level. In our study we limited our ocean-model domain to that used by Stammer (2008) to investigate the extra effect on the solution resulting from the coupling with the atmosphere. Any future extensions will need to include also the Arctic and its addition bridging effect into the Pacific.

Acknowledgements While revising this paper, Peter Herrmann, a co-author of this paper, unexpectedly passed away and we are indebted for his contribution to this paper. We thank R. Ray and S. Luthke for providing the Greenland mass loss field. CRM acknowledges financial support through the Deutsche Forschungs Gemeinschaft (DFG) funded excellence initiative CliSAP during several research visits to the University of Hamburg. we also thank several anonymous referees who provided very constructive and helpful comments. Funded in part through a MPG (Max Planck Society) Fellowship, the Special Research Program (SPP

1257) “Mass transports and distribution in the Earth System” funded by the DFG, and the BMBF (Federal Ministery of Education and Sciencr) Project REAL-GOACE. Contribution to the CliSAP Excellence Cluster, also funded through the DFG.

References

Agarwal N, Herrmann P, Mechoso CR, Köhl A, Stammer D (2011) Atmospheric response to high-latitude perturbations in the oceanic freshwater forcing. To be submitted for publication

Arakawa A, Schubert WH (1974) Interaction of a cumulus cloud ensemble with the large-scale environment, Part I. J Atmos Sci 31:674-701

Cazes-Boezio G, Menemenlis D, Mechoso CR (2008) Impact of ECCO Ocean-State Estimates on the Initialization of Seasonal Climate Forecasts. J Climate 21:1929-1947

Dorman JL, Sellers PJ (1989) A global climatology of albedo, roughness length and stomatal resistance for atmospheric general circulation models as represented by the Simple Biosphere Model (SiB). J Appl Meteor 28:833-855

Eden C, Greatbatch RJ (2003) A damped decadal oscillation in the North Atlantic climate system. J Climate 16:4043-4060

Gent PR, McWilliams JC (1990) Isopycnal mixing in ocean circulation models. J Phys Oceanogr 20:150-155

Greatbatch RJ (1994) A note on the representation of steric sea-level in models that conserve volume rather than mass. J Geophys Res 99:12767-12771

Harshvardhan, Randall DA, Corsetti TG (1987) A fast radiation parameterization for atmospheric circulation models. J Geophys Res 92:1009-1016

Harshvardhan, Corsetti TG, Dazlich DA (1989) Earth radiation budget and cloudiness simulations with a general circulation model. J Atmos Sci 46:1922-1942

Hawkins E, Sutton R (2009) Decadal predictability of the Atlantic Ocean in a coupled GCM: forecast skill and optimal perturbations using Linear Inverse Modelling. J Climate. doi: 10.1175/2009JCLI2720.1

Hu A, Meehl GA, Han W, Yin J (2009) Transient response of the MOC and climate to potential melting of the Greenland Ice Sheet in the 21st century. Geophys Res Lett. doi:10.1029/2009GL037998

Köhler M (1999) Explicit prediction of ice clouds in general circulation models. Ph.D. Dissertation, Department of Atmospheric Sciences, University of California, Los Angeles

Kopp RE, Mitrovica JX, Griffies SM, Yin J, Hay CC, Stouffer RJ (2010) The impact of Greenland melt on local sea levels: a partially coupled analysis of dynamic and static equilibrium effects in idealized water-hosing experiments. Clim Change. doi:10.1007/s10584-010-9935-1

Konor CS, Cazes-Boezio G, Mechoso CR, Arakawa A (2008) Parameterization of PBL processes in an Atmospheric General Circulation Model: Description and Preliminary Assessment. Mon Wea Rev 137(3):1061

Large WG, McWilliams JC, Doney S (1994) Oceanic vertical mixing: A review and a model with a nonlocal boundary layer parameterization. Rev Geophys 32:363-403

Landerer FW, JH Jungclaus, L Marotzke (2007) Regional dynamic and steric sea level change in response to the IPCC-A1B scenario. J Phys Oceanogr 37:296-312

Large WG, Danabasoglu G, Doney SC, McWilliams JC (1997) Sensitivity to surface forcing and boundary layer mixing in a global ocean model: Annual-mean climatology. J Phys Oceanogr 27:2418-2447

Li, JL, Köhler, M, Farrara JD, Mechoso CR (2002) The impact of stratocumulus cloud radiative properties on surface heat fluxes simulated with a general circulation model. Mon Wea Rev 130:1433-1441

Luthke S, Zwally H, Abdalati W, Rowlands DD, Ray RD, Nerem RS, Lemoine FG, McCarthy JJ, Chinn DS (2006) Recent Greenland mass loss by drainage system from satellite gravity observations. Science 314(5803):1286-1289

Ma HY, Mechoso CR, Xue Y, Xiao H, Wu CM, Li JL, DeSales F (2010) Impact of land surface processes on the South American warm season climate. Clim Dyn. doi:10.1007/s00382-010-0813-3

Mitrovica JX, Tamisea MW, Davis JL, Milne GA (2001) Recent mass balance of polar ice sheets inferred from pattern of global sea level change. Nature 409:1026-1029

Okumora YM, Deser C, Hu A (2009) North Pacific Climate Response to Freshwater focring in the subarctic North Atlantic: oceanic and atmospheric pathways. J Clim. doi:10.1175/2008JCLI2511.1

Pan DM, Randall DA (1998) A cumulus parameterization with a prognostic closure. Quart J Roy Met Soc 124:949-981

Pardaens A, Gregory JM, Lowe J (2010) A model study of factors influencing projected changes in regional sea level over the twenty-first century. Climate Dyn. doi:10.1007/s00382-009-0738-x

Rahmstorf S, Willebrand J (1995) The role of temperature feedback in stabilizing the thermohaline circulation. J Phys Oceanogr 25:787-805

Rahmstorf S, Crucifix M, Ganopolski A, Goosse H, Kamenkovich I, Knutti R, Lohmann G, Marsh R, Mysak LA, Wang Z, Weaver AJ (2005) Thermohaline circulation hysteresis: A model intercomparison. Geophys Res Lett. doi:10.1029/2005GL023655

Redi MH (1982) Oceanic isopycnical mixing by coordinate rotation. J Phys Oceanogr 12:1154-1158

Stammer D (2008) Response of the global ocean to Greenland and Antarctic ice melting. J Geophys Res. doi:10.1029/2006JC004079

Stouffer RJ, Yin J, Gregory JM, Dixon KW, Spelman MJ et al (2006) Investigating the causes of the response of the thermohaline circulation to past and future climate changes. J Clim 19:698-722

Suarez M, Arakawa A, Randall D (1983) The parameterization of the planetary boundary layer in the UCLA general circulation model: Formulation and Results. Mon Wea Rev 111:2224-2243

Timmermann A, Okumura Y, An SI, Clement A, Dong B, Guilyardi E, Hu A, Jungclaus JH, Renold M, Stocker TF, Stouffer RJ, Sutton R, Xie SP, Yin J (2007) The Influence of a Weakening of the Atlantic Meridional Overturning Circulation on ENSO. J Clim. doi:10.1175/JCLI4283.1

Xue Y, Sellers PJ, Kinter III JL, Shukla J (1991) A simplified biosphere model for global climate studies. J Clim 4:345-364

Xue Y, Bastable HG, Dirmeyer PA, Sellers PJ (1996a) Sensitivity of simulated surface fluxes to changes in land surface parameterization - a study using ABRACOS data. J Appl Met 35:386-400

Xue Y, Fennessy MJ, Sellers PJ (1996b) Impact of vegetation properties on US summer weather prediction. J Geophys Res 101:7419-7430

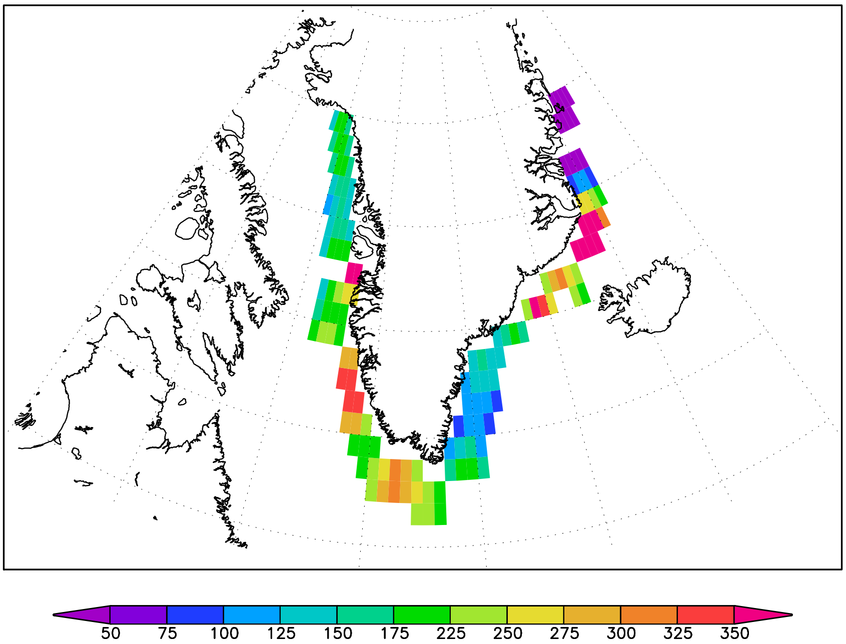

Fig. 1 Surface freshwater flux anomalies (in m^3/s) equivalent to 5 times the recent ~170 GT per annum (Luthke 2006) estimates of Greenland melt water loss.

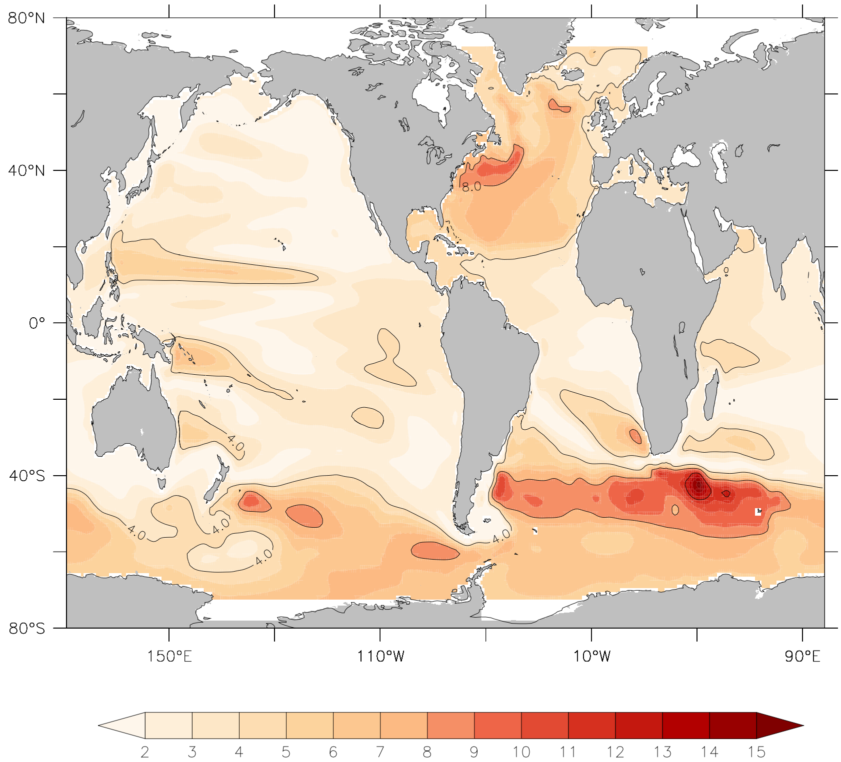

Fig. 2 Standard deviation (in cm) of the lowpass filtered (5-year running mean) sea surface height variations of the CGCM reference run over the 50-year integration period. Solid contour lines correspond to levels of 4 cm and 10 cm. The global mean is 3.97 cm.

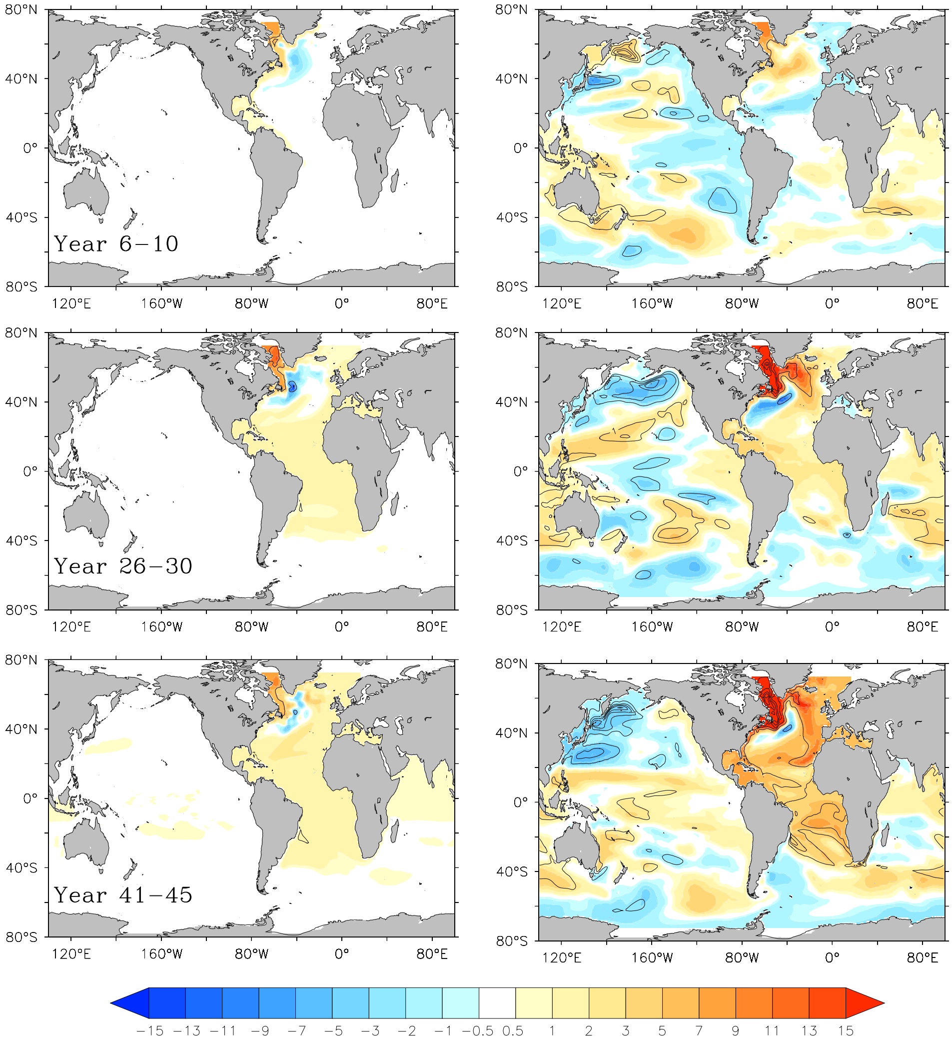

Fig. 3 Lowpass filtered SSH anomalies from the uncoupled (left column) and coupled (right column) experiments averaged over the years 6-10 (top), 26-30 (middle) and 41-45 (bottom), respectively. Units are cm, using a white-centered nonlinear color-scale. In the right column, contours mark statistically significant areas (at a 65% confidence level and higher) using as a measure the quantity $|SSH - anomaly|/STD$ with a contour interval of 1. The respective STD field is shown in Fig. 2.

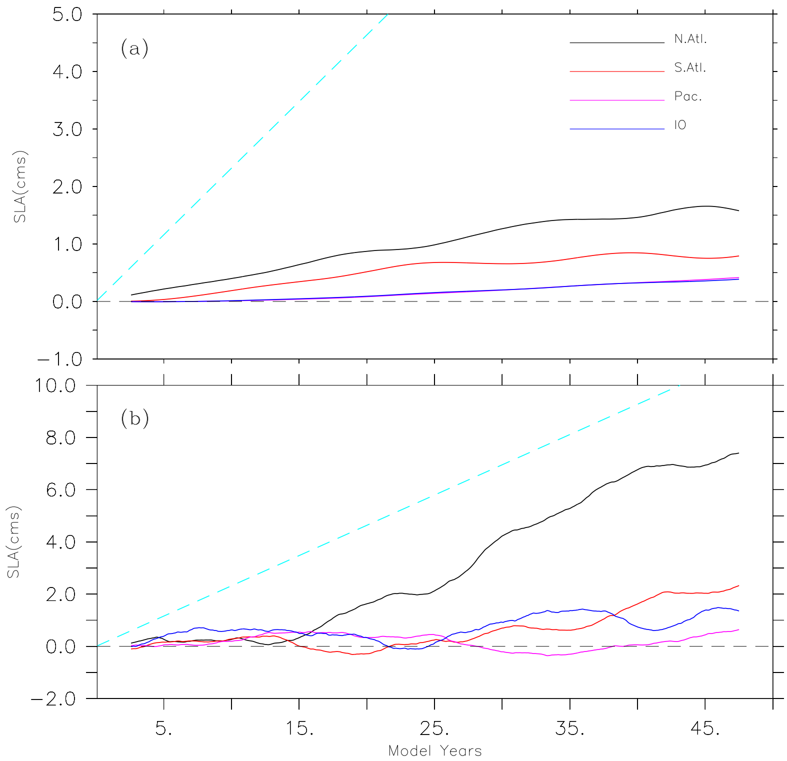

Fig. 4 Time series of lowpass filtered steric SSH anomalies (cm) (using a 5-year running mean) averaged over different ocean basins from ocean-only (top) and coupled (bottom) runs. Dashed blue line represents the non-steric sea level increase due to the meltwater addition. The curves labeled Pac. and IO represent the Pacific Ocean and the Indian Ocean respectively; they overlap in the top panel.

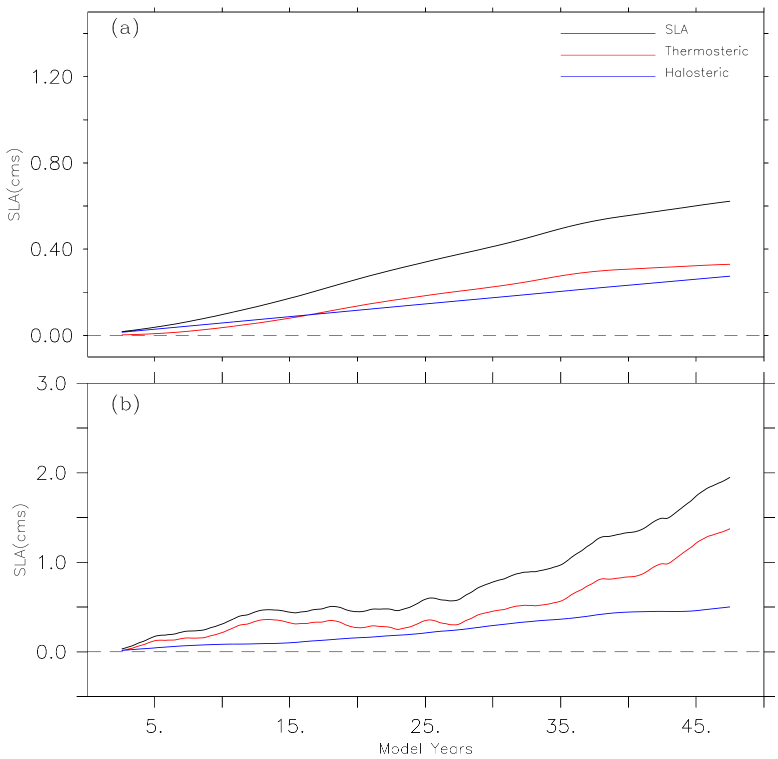

Fig. 5 Time series of globally averaged lowpass-filtered steric SSH anomalies (SLA; black in cm) and contributions from thermosteric (red line) and halosteric (blue line) effects ocean-only (top) and coupled (bottom).

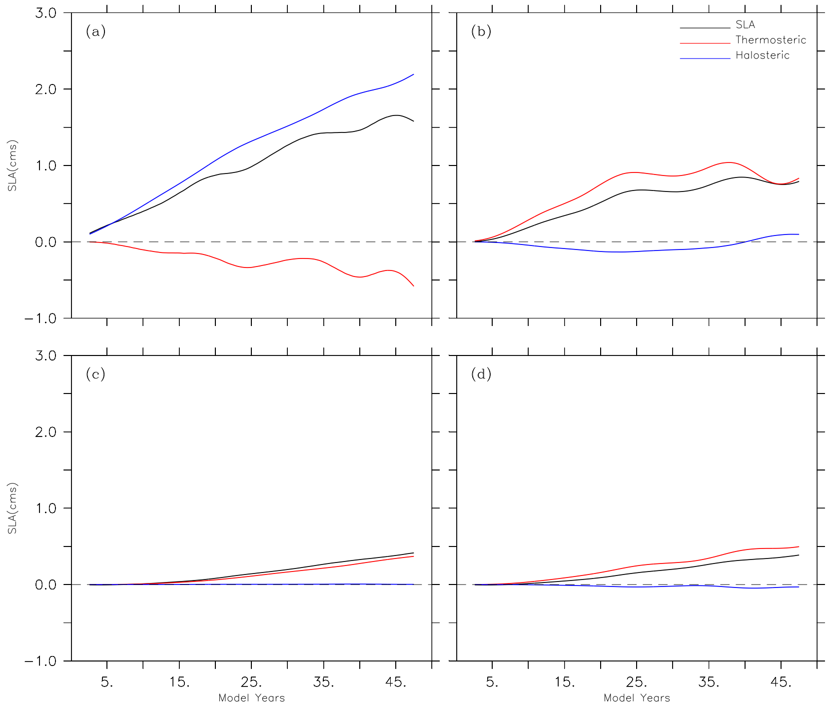

Fig. 6 Time series of basin averaged lowpass-filtered steric SSH anomalies(SLA, black in cm) and contributions from thermosteric (red line) and halosteric (blue line) effects in (a) North Atlantic, (b) South Atlantic, (c) Pacific and (d) Indian Ocean as seen in the uncoupled runs.

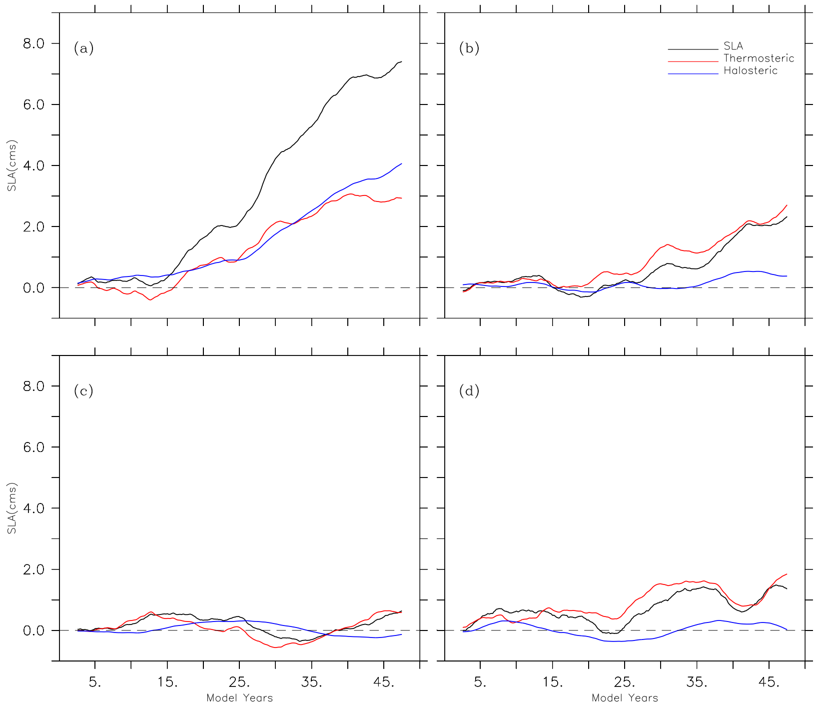

Fig. 7 Same as Fig. 6, but from coupled runs.

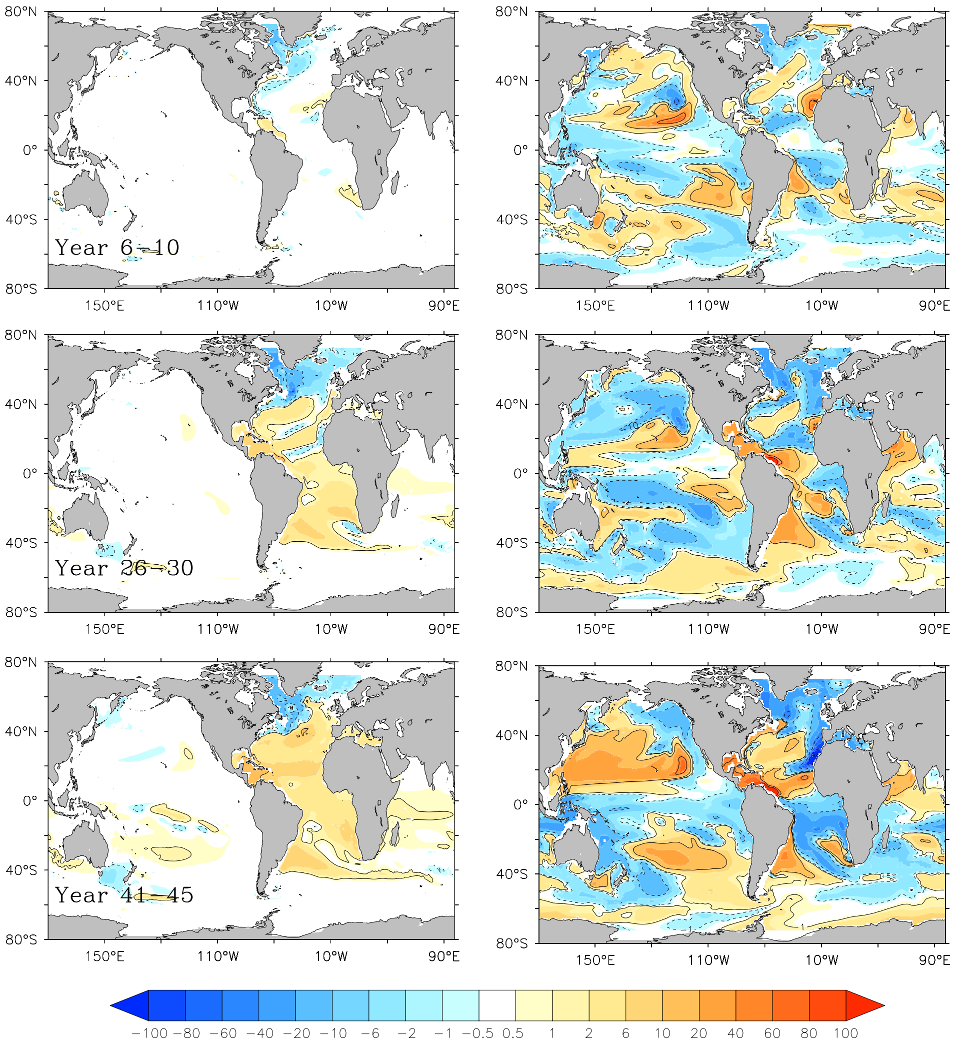

Fig. 8 Maps of mean salinity anomalies at 160m depth resulting from the uncoupled (left column) and coupled (right column) experiments after lowpass-filtering (5-year running mean), each averaged over years 6-10 (top), 26-30 (middle) and 41-45 (bottom), respectively. Units are 0.01 PSU, using a white centered nonlinear colorscale. Contours on top are between $\pm 100 \times 10^{-2}$ psu at an interval of 50×10^{-2}, between $\pm 10 \times 10^{-2}$ at an interval of 10×10^{-2}, and between $\pm 1 \times 10^{-2}$ at an interval of 1×10^{-2}, excluding 0.

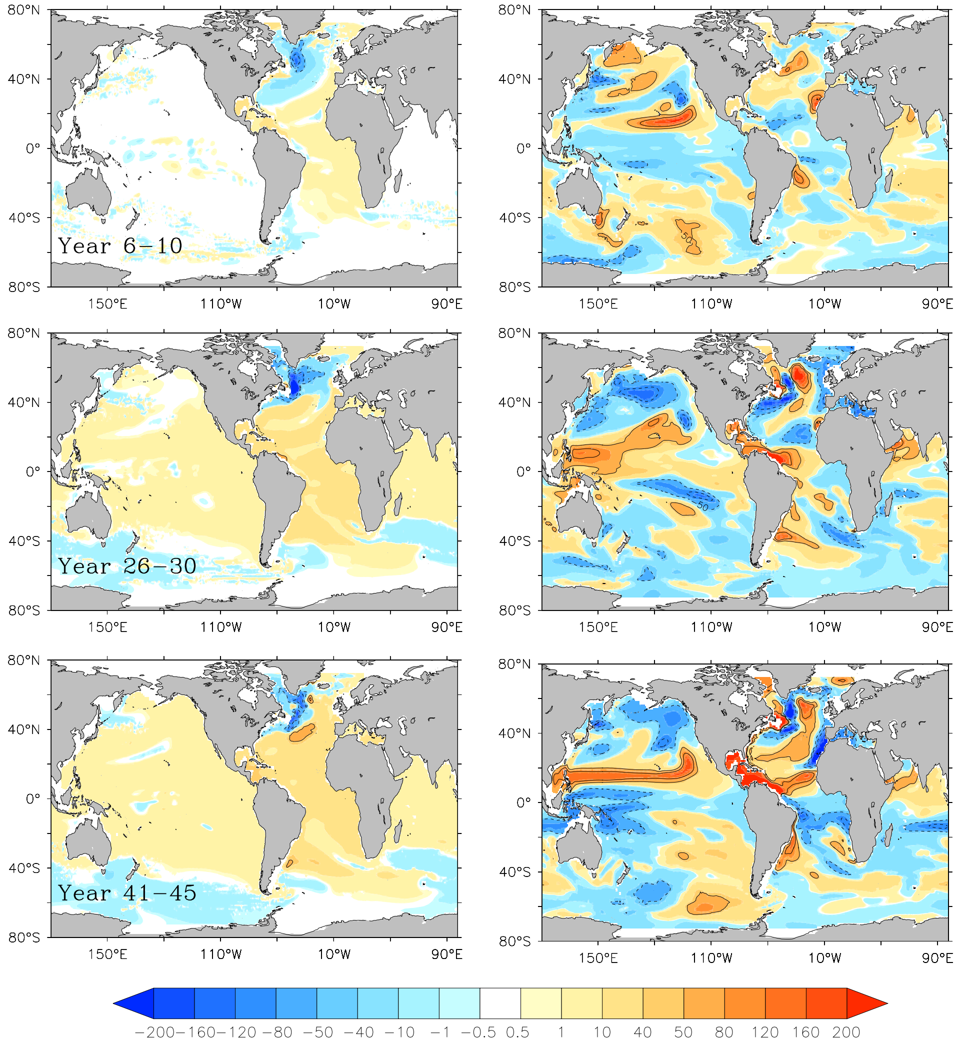

Fig. 9 Maps of mean temperature anomalies at 160m depth resulting from the uncoupled (left column) and coupled (right column) experiments after lowpass-filtering (5-year running mean), each averaged over years 6-10 (top), 26-30 (middle) and 41-45 (bottom), respectively. Units are 0.01 °C. Using a white centered nonlinear colorscale. Contours on top are between $\pm 100 \times 10^{-2}$ °C at an interval of 50×10^{-2} °C, excluding 0.

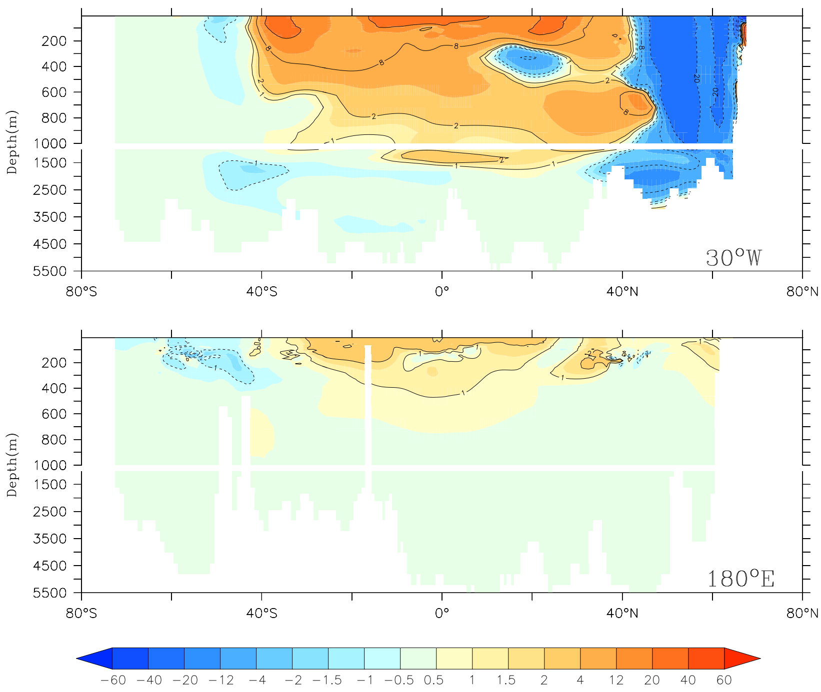

Fig. 10 Meridional cross section of lowpass filtered temperature anomalies (in 10^{-2} °C) at (upper panel) 30°W and (lower panel) 180°E, both averaged over the 50-year long uncoupled runs.

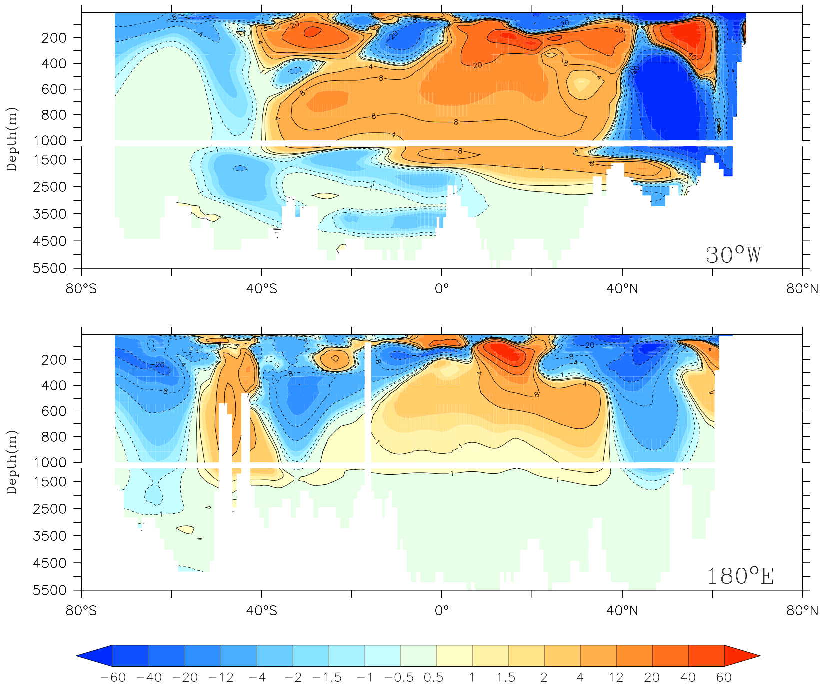

Fig. 11 Meridional cross section of lowpass filtered temperature anomalies (in 10^{-1} °C) at (upper panel) 30°W and (lower panel) 180°E averaged over the 50-year long coupled runs.

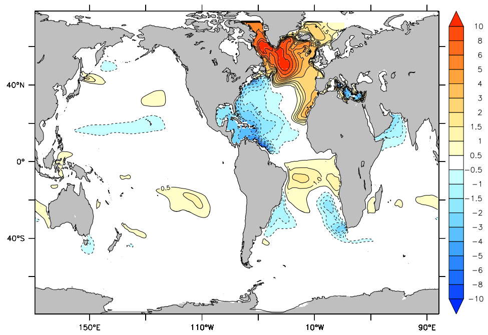

a

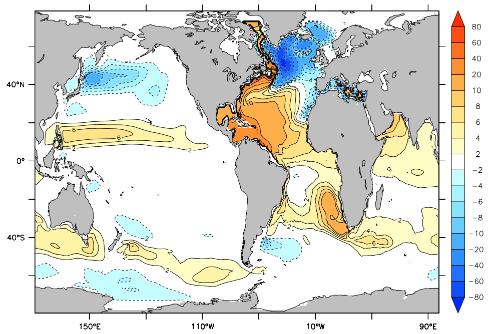

b

Fig. 12 50-year mean anomalies of (top) freshwater content (m) and (bottom) heat content ($10^8 J/m^2$).

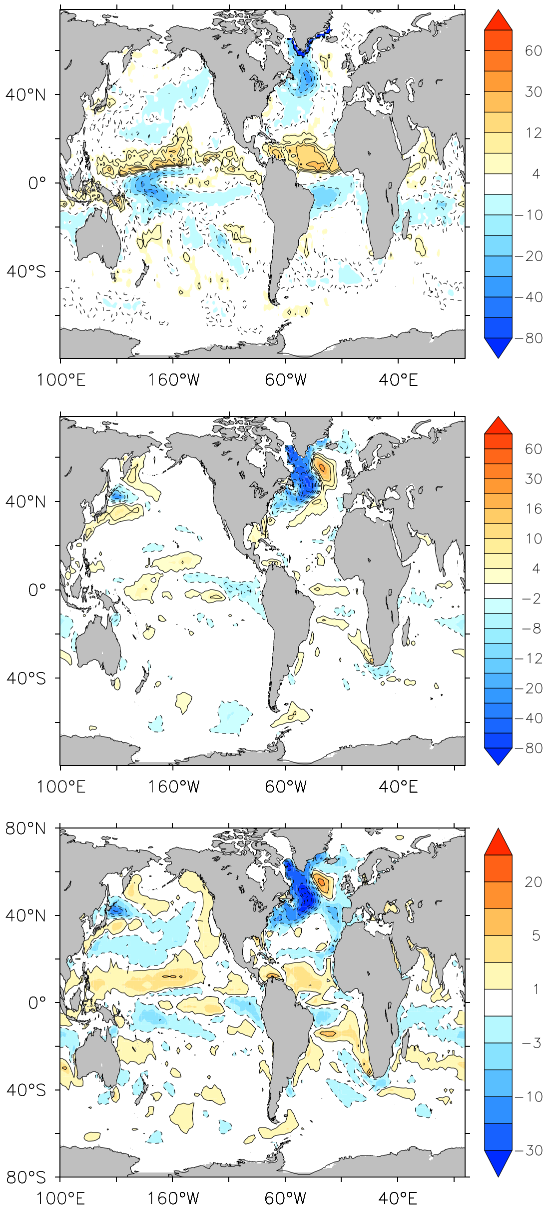

Fig. 13 Mean changes in (top) net freshwater flux ($cm/year$), and (middle) net surface heat flux (W/m^2) in the coupled run averaged over the 50 year period. Contours on top of latent heatflux anomalies are -50 to 50 W/m^2 with an interval of 10, -10 to 10 with an increment of 5 and -1 to 1 with an increment of 2, all excluding the zero line. (bottom) 50 year averaged difference in latent heatflux, using a contour interval of 2 W/m^2 over a range of $\pm$ 30 W/m^2.

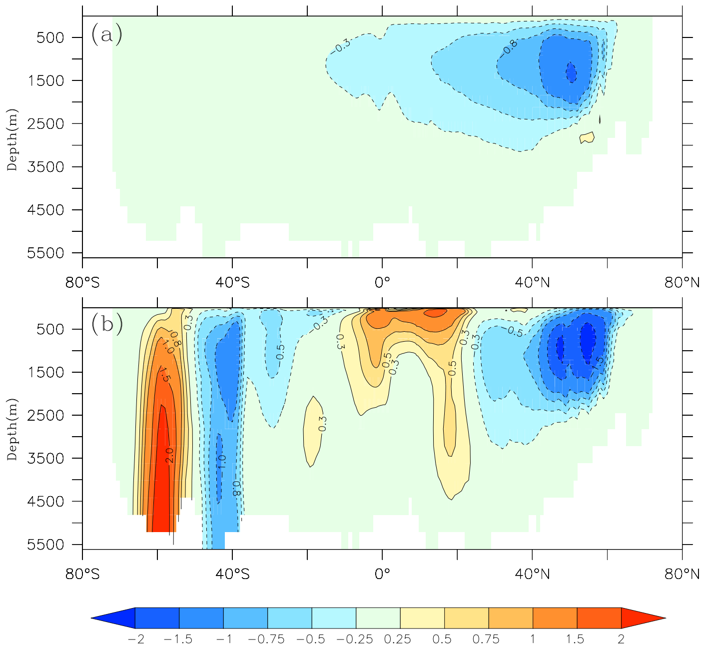

Fig. 14 Examples of annual mean anomalies of the MOC (Sv) taken randomly from year 8 from (top) uncoupled and (bottom) coupled runs.

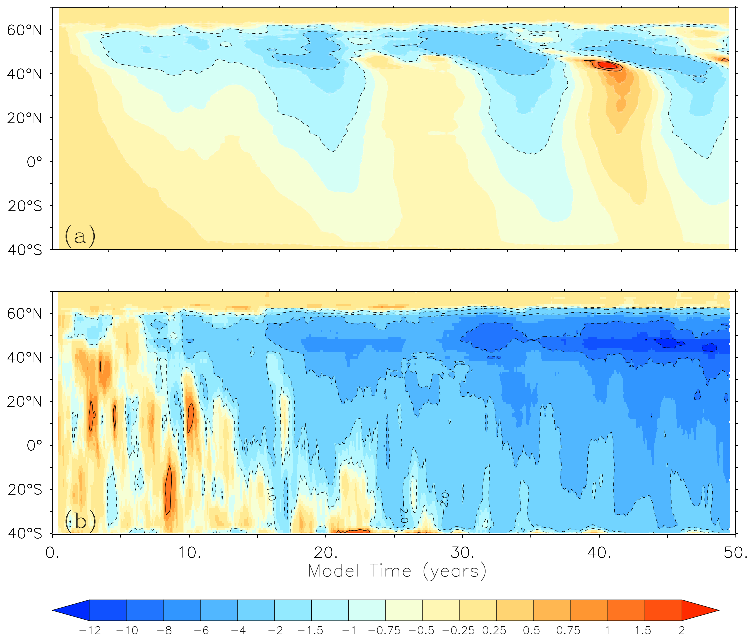

Fig. 15 Time-latitude plot of MOC anomaly (Sv) at 1000 m depth from (top) uncoupled and (bottom) coupled runs.

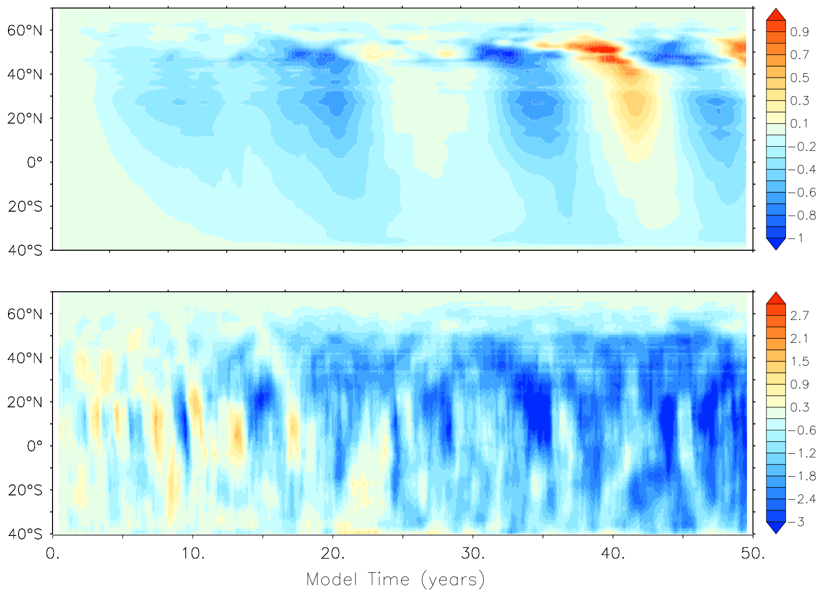

Fig. 16 Time-latitude plot of the meridional heat transport anomaly (PW) from (top) uncoupled and (bottom) coupled runs.